

Article

Influence of Cylindrical Cells Surface Cleaning by Means of Laser Ablation on Wedge Wire Bonding Process

Krzysztof Bieliszczuk ^{1,*} , Jakub Zręda ² and Tomasz M. Chmielewski ¹ 

¹ Department of Joining Engineering, Faculty of Mechanical and Industrial Engineering, Warsaw University of Technology, Narbutta 85, 02-524 Warsaw, Poland; tomasz.chmielewski@pw.edu.pl

² evHive Jakub Zręda, 05-500 Józefosław, Poland

* Correspondence: krzysztof.bieliszczuk@pw.edu.pl

Abstract: Wire bonding is a method of connecting two or more surfaces by the means of a thin wire which is ultrasonically bonded to those surfaces and provides an electrical connection. While this method is well established in the microelectronics industry its popularity is rising in the area of cylindrical lithium-ion battery pack manufacturing. Previous studies have shown that even in experimental conditions this process might be unstable which was indicated by the high standard deviation of the bonds shear test results. This might have been related to contamination of the interface area between the joined materials. The aim of this study was to determine the impact of surface laser cleaning on the properties of the wire-bonded joint. The results have shown that laser cleaning with 40% power of the 30 W ATMS4060 laser marker helps to reduce the standard deviation of the shear test results from 16.1% for the uncleaned sample down to 2.6% and greatly reduces the number of oxides within the interface area of the bond cross section. Cleaning with 80% of the laser power did not have a further impact on shear test results and almost completely eliminated oxides from the bonded materials interface.

Keywords: surface preparation; beam cleaning; wire bonding; battery cell; ultrasonic bonding



Citation: Bieliszczuk, K.; Zręda, J.; Chmielewski, T.M. Influence of Cylindrical Cells Surface Cleaning by Means of Laser Ablation on Wedge Wire Bonding Process. *Coatings* **2024**, *14*, 445. <https://doi.org/10.3390/coatings14040445>

Academic Editor: Roberto Teghil

Received: 21 March 2024

Revised: 5 April 2024

Accepted: 6 April 2024

Published: 9 April 2024



Copyright: © 2024 by the authors. Licensee MDPI, Basel, Switzerland. This article is an open access article distributed under the terms and conditions of the Creative Commons Attribution (CC BY) license (<https://creativecommons.org/licenses/by/4.0/>).

1. Introduction

Wire bonding is a method of making electrical interconnections by the means of a metal wire that is ultrasonically bonded to two or more surfaces. It is a solid-state welding process characterized by low diffusion of bonded materials [1], relying mostly on adhesion. The method of wire bonding most commonly used in the battery industry is heavy wedge wire bonding [2]. This method uses a sonotrode that has a v-shaped groove in which the bonding wire is located. Connection is made by applying a set force to push the wire material into the substrate and then applying ultrasonic vibrations to create a permanent joint. Materials used for the bonding wires are most commonly pure or alloyed aluminum, copper, gold, and silver [3]. In battery pack manufacturing aluminum, copper, and aluminum-coated copper wires are used with diameters ranging from 100 to 500 μm . Previous studies have proven that the wire bonding process stability, in particular the mechanical strength of the joint is not repeatable for out-of-the-box cylindrical cells [4]. The aim of this study is to analyze the dependency between selected joint properties and the state of the battery cell surface. The method selected for surface preparation was laser cleaning due to its low cost, high availability, and ease of implementation.

Wire bonding itself is a self-cleaning process [5,6] that expels impurities from the interface area by the means of heat, plastic deformation, and ultrasonic vibrations resulting in the shearing of the material [7,8]. Surface cleaning prior to wire bonding has been proven to enhance the properties of the resulting joint in the process of bonding on silicon-based substrates used widely in the semiconductor industry [9]. Although wire bonding is widely used in the battery industry [10], studies on surface cleaning of nickel-plated steel used

for cylindrical battery shell production in the aluminum wire bonding process are not widely available.

Methods of surface preparation include mechanical cleaning with solvents [11], laser cleaning [12–14], CO₂ cleaning [15], and plasma cleaning [16]. Cleaning with solvents and chemicals is a lengthy process not suitable for large-scale production. CO₂ cleaning is an advanced process requiring costly equipment and development work suitable for the semiconductor industry, but it is not cost-efficient for manufacturing battery packs. The plasma cleaning process of the battery cells poses a risk of damage to the battery isolator and did not gain popularity in battery surface cleaning. Laser cleaning is the most commonly used method of cleaning battery cells prior to bonding due to low cost, high precision of the laser beam, the ability to program complex geometries for the cleaned area, and relatively low process time. Various dedicated laser cleaning machines are available on the market. Dedicated systems are usually expensive solutions in comparison to multi-purpose marking systems implementing low-power fiber lasers. This has posed the question of whether it is indeed necessary to invest in a dedicated laser cleaning system and led us to conduct preliminary tests using both solutions. Those tests have shown the feasibility of implementing a laser cleaning process using a low-cost 30 W laser marking system and therefore this type of machine was used in further study.

2. Materials and Methods

The parameters and equipment used for the wire bonding process in this study are identical to our previous research which revealed the high distribution of the results of shear testing [4]. Please refer to that study for a more detailed description of the process.

This study uses Heraeus Holding GmbH (Hanau, Germany) 400 µm AluBond Pure H11 aluminum wire and BAK Battery Co., Ltd. (Shenzhen, China) N18650CP BAK A02 lithium-ion cylindrical battery cells. Bonds have been placed on the battery cap which is the positive terminal of the battery cell as seen in Figure 1.



Figure 1. Wire bond visible on battery cap after cutting off top of battery cell.

The chemical composition of the AluBond Pure H11 wire as provided by the manufacturer (Heraeus) has been presented in Table 1 while its mechanical properties have been presented in Table 2.

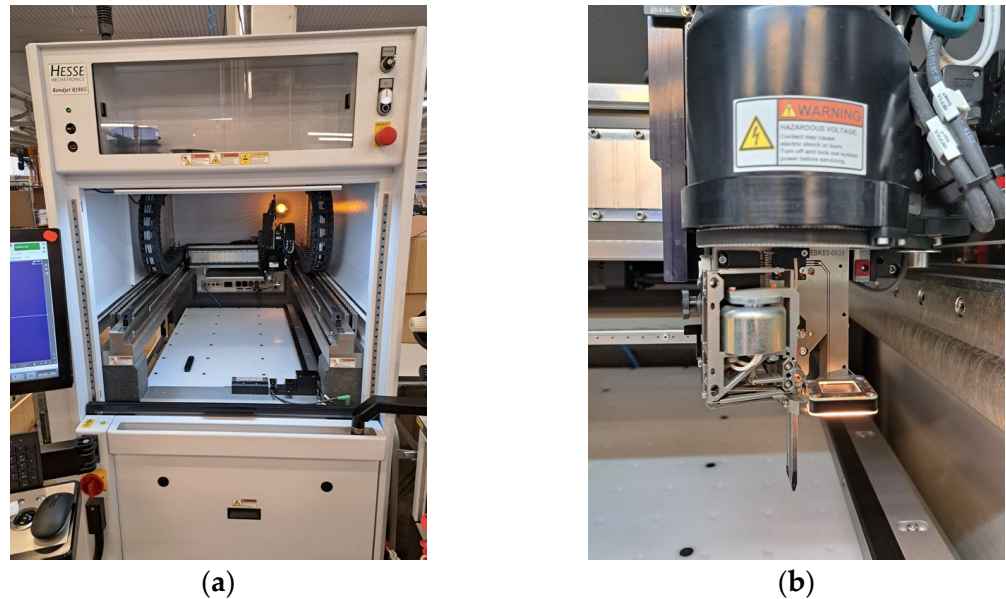
Table 1. Chemical composition (wt.%) of AluBond Pure H11 bonding wire (Heraeus specification).

	Al	Cu	Si	Fe
Tested	99.99919	0.00040	0.00030	0.00011
Spec limit	≥99.99700	≤0.00180	≤0.00050	≤0.00200

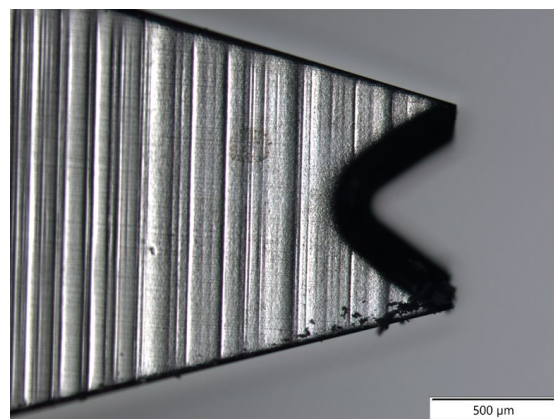
Table 2. Mechanical properties of AluBond Pure H11 bonding wire (Heraeus specification).

	Breaking Load [cN]	Elongation Limit [%]
Tested	576.1	17.7
Spec limit	500.0–670.0	>5.0

The machine used for bonding was a Hesse GmbH (Paderborn, Germany) BJ985 wire bonder as seen in Figure 2a equipped with RBK03 bondhead seen in Figure 2b [4].

**Figure 2.** Hesse BJ985 wire bonder (a) and RBK03 bondhead (b) [4].

Sonotrode used in this study was Hesse model 65408-400 as seen in Figure 3. Sonotrode is made out of tungsten carbide and its resonance frequency is 58 kHz.

**Figure 3.** Sonotrode wedge Hesse 65408-400.

Wire bonding process parameters can be described in 3 phases as seen in Figure 4. The force plot represents the force that the bondhead is pressing the wire material into the substrate. The ultrasonic current represents the current supplied to the ultrasonic generator. This process is controlled to achieve a constant set current as for the bonding parameters plot. This is achieved by changing the voltage of the ultrasonic generator power supply. Touchdown is a phase prior to bonding in which the wire is being pushed into the substrate without ultrasonic oscillations. The time of the whole bonding process is 500 ms.

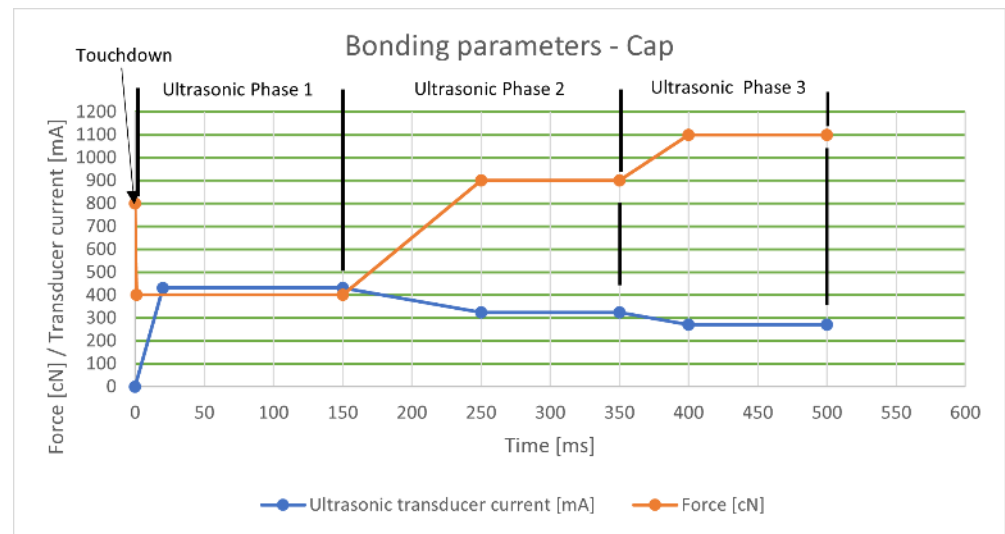


Figure 4. Bonding process parameters.

The laser cleaning process has been conducted on a Fiber ATMS 4060 laser manufactured by ATMSolutions Sp.z o.o. (Łomianki, Poland). Laser specification has been presented in Table 3 and the parameters of the laser cleaning process have been presented in Table 4. Throughout the study, the only variable parameter was the laser source power. Samples for each parameter set were laser cleaned and then immediately bonded. No correction of focus height or sample location has been conducted between the samples.

Table 3. Fiber ATMS 4060 laser specifications.

Parameter	Value
Laser source type	Fiber
Laser power	30 W
Laser wavelength	1060 nm
Laser source max frequency	100 kHz
Lens size	300 × 300 mm

Table 4. Laser cleaning parameters were used in this study.

Parameter	Value	Description
Speed	2000 mm/s	Speed of the laser beam
Power	0/20/40/80%	Power of the laser (pulse modulation)
Start TC	−100 μs	Time between mirror movement and laser on
Laser off TC	300 μs	Time between mirror stop and laser stop at program end
End TC	300 μs	Time between mirror stop and laser stop at polygon end
Polygon TC	100 μs	Time wait in vector connection point of polygon
Line space	0.01 mm	Distance between consecutive laser lines
Frequency	20 kHz	Laser source switching frequency

Cross section samples for microscopy were mounted in ATM Qness GmbH (Mammelzen, Germany) DUROPLAST electroconductive hot mounting powder and grinded using #80, 200, 400, 800, 1200, and 2000 silicon carbide papers. Polishing was conducted using Struers S.A.S. (Champigny-sur-Marne, France) DiaPro Nap 5 μm diamond solution followed by Struers OP-S 0.25 μm colloidal silica solution.

Samples were analyzed using an Olympus (Tokyo, Japan) SZ61 light microscope for macroscopic investigation, an Olympus BX51M light microscope for microscopic investigation, Thermo Fisher Scientific Inc. (Waltham, MA, USA) Axia ChemiSEM Scanning Electron Microscope (SEM) for electron microscopy, and Energy Dispersive Spectroscopy (EDS).

Shear testing was conducted according to DVS-2811 on XYZtec bv (Panningen, The Netherlands) Sigma tester using a rotating 1.2 mm shear tool. Testing parameters have been presented in Table 5 while sample location during testing can be seen in Figure 5.

Table 5. Shear test parameters.

Parameter	Value	Description
Test distance	800 μm	Shear tool travel during testing
Test speed	100 $\mu\text{m}/\text{s}$	Speed of the shear tool
Touchdown force	20 cN	Force required for substrate surface detection
Shear height	40 μm	Height from substrate level at which shear test takes place

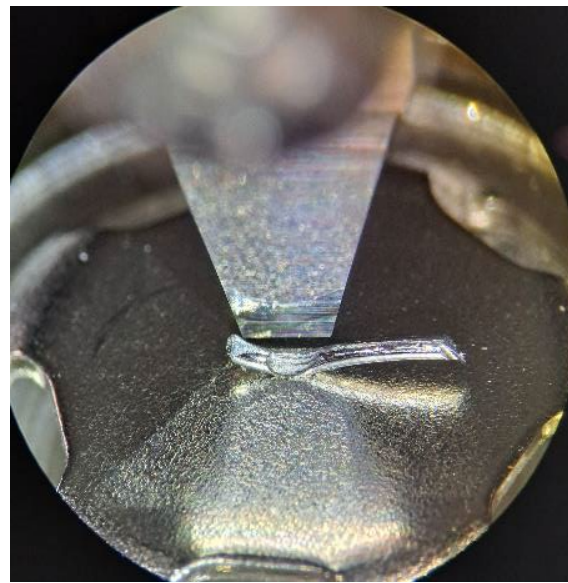


Figure 5. Shear tool location during testing follows the same formatting.

The shear test takes place with the battery located in the bonding holder that is secured in the shear tester vice. The shear tool is manually moved and rotated to face the bond about 100 μm from the side of the wire. An automatic test is initiated, and the shear tool moves down to detect the height of the substrate. Then the shear tool moves up 40 μm (10% of the wire diameter) from the detected surface and begins its test movement toward the bond.

Optical macroscopy after shear testing has been conducted in order to determine the failure mode of the connection.

3. Results

Results can be divided into four subsections: Light microscopy and SEM investigation of laser-cleaned surface, SEM investigation of bond cross sections, and shear test results.

3.1. Microscopy of Laser Cleaned Surface

In order to determine whether the laser cleaning process had any impact on the substrate surface optical microscopy was conducted for samples cleaned with 20, 40, and 80% of the laser power.

As seen in macroscopic images presented in Figure 6 there is no noticeable difference between a surface cleaned with 20% laser power and an uncleaned surface. This allowed us to exclude this power of laser cleaning from further studies.

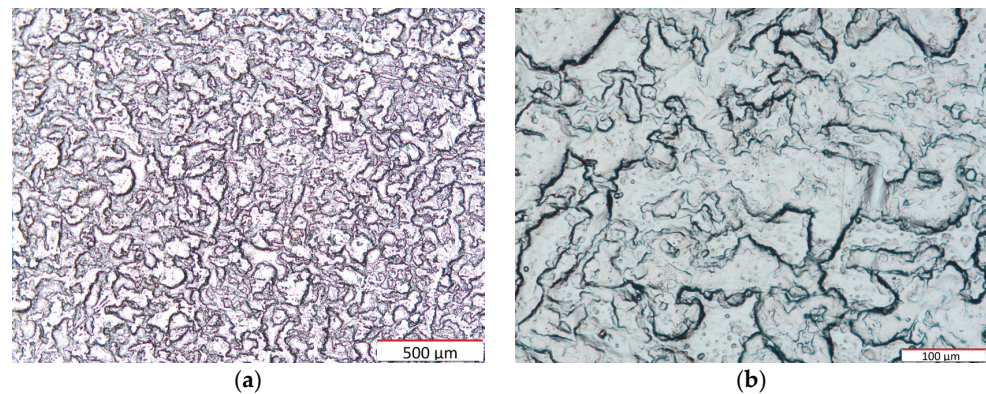


Figure 6. Boundary of the cleaned surface $\times 50$ (a) and $\times 200$ (b) magnification for 20% laser cleaning power.

Figure 7 shows the boundary of the laser cleaning process for 40% laser power. The boundary is clearly noticeable as the area outside the laser-cleaned zone (top right) is less reflective than the cleaned area (bottom left). This indicates that the cleaning parameters used for this sample are having an effect on the substrate surface and should be analyzed further.

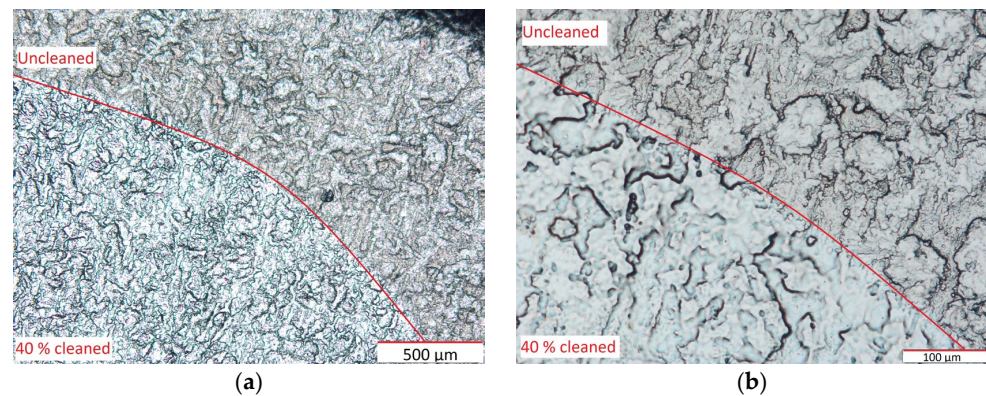


Figure 7. Boundary of the cleaned surface $\times 50$ (a) and $\times 200$ (b) magnification for 40% laser cleaning power.

Figure 8 shows the boundary between the uncleaned surface (top) and the 80% laser-power cleaned surface (bottom). In this case not only the reflectiveness of the surface changed, but also its structure. This indicates that the surface has been locally raised above its melting point. Those parameters should also be investigated further.

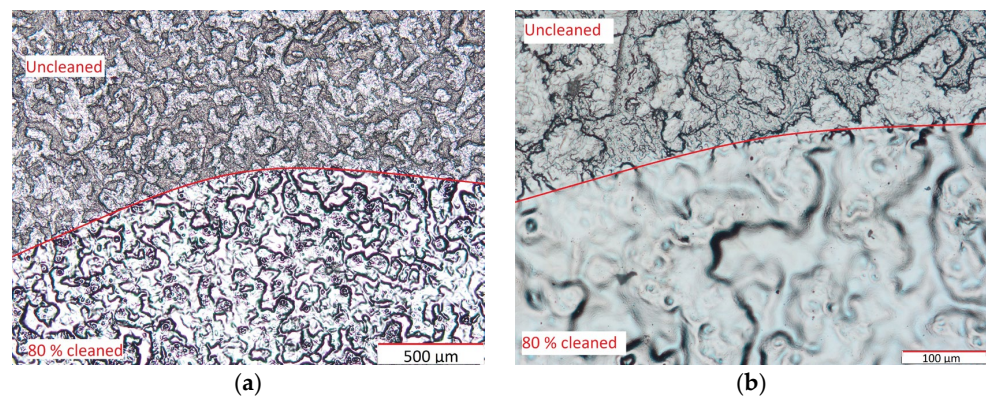


Figure 8. Boundary of the cleaned surface with $\times 50$ (a) and $\times 200$ (b) magnification for 80% laser cleaning power.

3.2. SEM Investigation of Laser Cleaned Surface

The surfaces of battery cells were analyzed by SEM and EDS to determine the influence of the laser cleaning parameters on the bonding substrate.

Results of SEM show, that there are many impurities visible on the sample that were not laser cleaned as seen in Figure 9a. Samples cleaned with 20% (Figure 9b) and 40% (Figure 9c) of the laser power do not have the same impurities, that were observed on the uncleaned sample but appear to be similar in surface structure. The sample cleaned with 80% of the laser power visible in Figure 9d has a visibly changed surface structure. Observed semicircular marks were spots where the laser beam had heated the surface of the sample. This indicates that at least a part of the nickel plating on the battery cell might have been ablated and the remaining material has been liquified in the process.

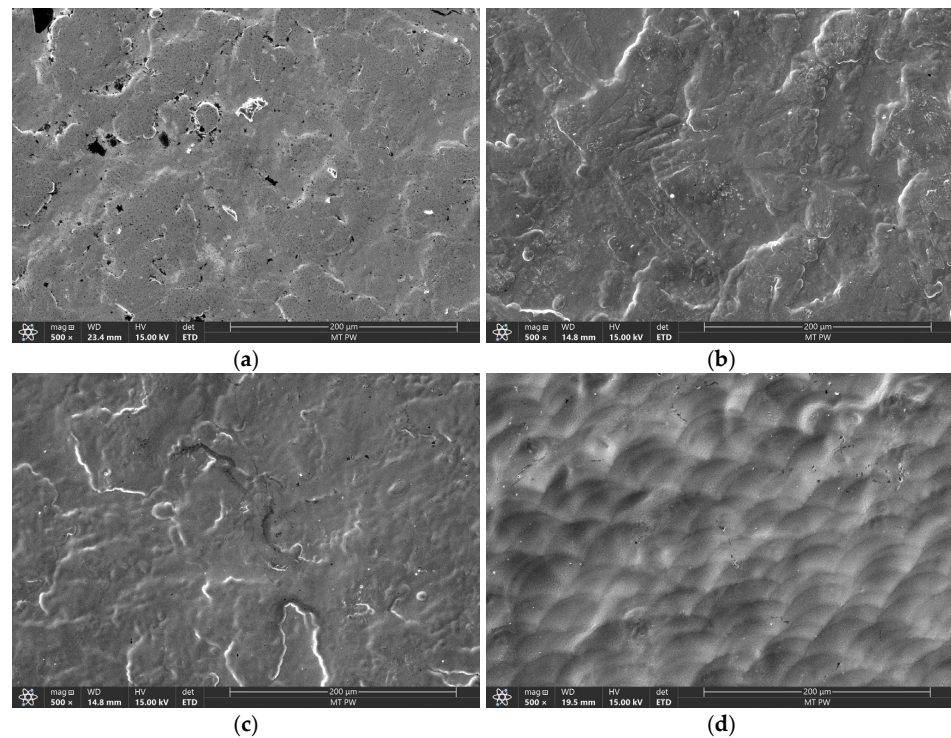


Figure 9. SEM imaging of the battery surface with 500× magnification for uncleaned (a), 20% (b), 40% (c), and 80% (d) laser power cleaned samples.

EDS analysis revealed that the sample cleaned with 80% of the laser power visible in Figure 10b has a uniform distribution of elements throughout the sample. Detected elements consists of carbon, nickel, iron, oxygen, and silicon. Uncleaned sample EDS results seen in Figure 10a revealed contamination of the surface with large particles of iron.

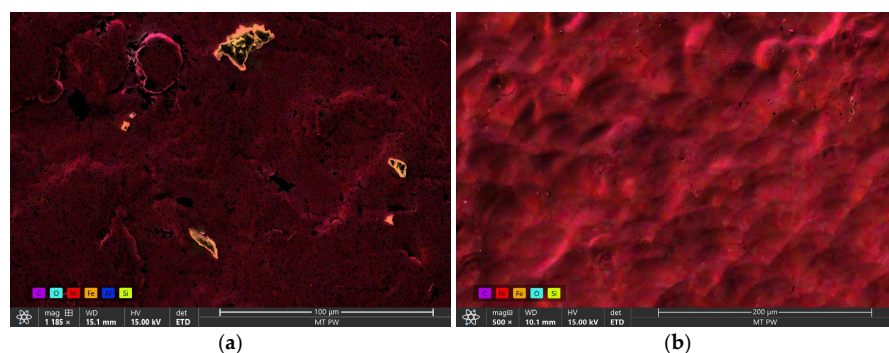


Figure 10. Comparison of EDS quantity map of the uncleaned (a) surface and surface cleaned with 80% laser power (b).

Distribution maps of elements visible in Figure 11 revealed large particles of iron visible on the sample surface. Patches containing heightened concentrations of carbon and oxygen have also been observed. Aluminum has also been detected in this sample in the same area as one of the foreign iron particles. Those results show that during the laser cleaning process, both types of contaminations—carbon and oxygen compounds and foreign metallic particles, are successfully removed.

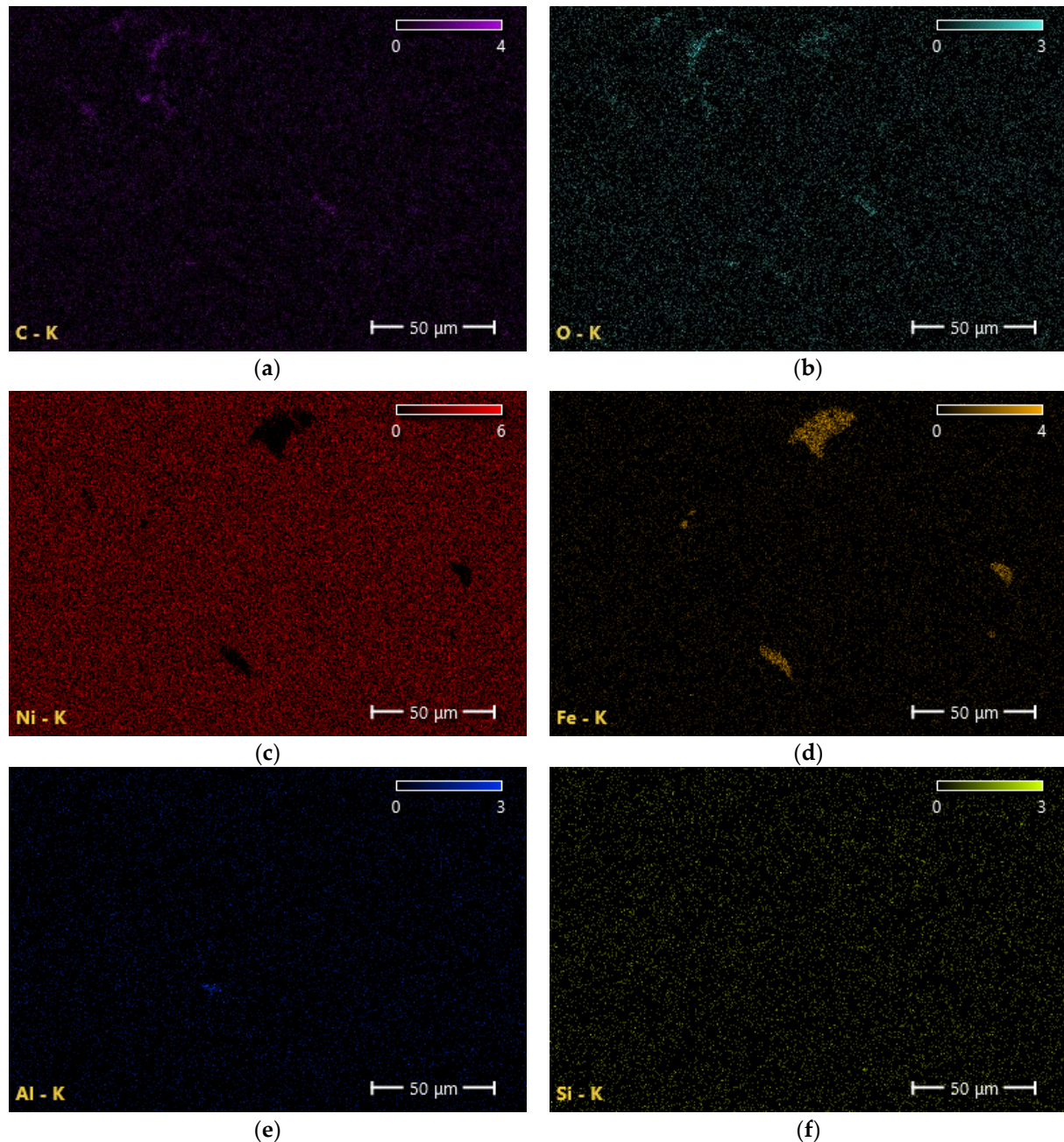


Figure 11. EDS count map of the uncleaned surface with distribution of carbon (a), oxygen (b), nickel (c), iron (d), aluminum (e), and silicon (f).

3.3. SEM Investigation of Bond Cross Section

For further studies, parameters of 40 and 80% of the laser power were selected and compared to the uncleaned sample. Bonds were made on each of the samples in order to determine the influence of the substrate surface state on the interconnection made during the wire bonding process.

Cross sections of the bond made on the surface that was not laser cleaned seen in Figure 12a–c revealed a poor connection between the aluminum wire and the surface of the battery cell. Many gaps were observed in the area of the materials interface. The aluminum wire has been deformed to the shape of the substrate, but the connection did not occur. EDS has been performed on the cross section as seen in Figure 12d.

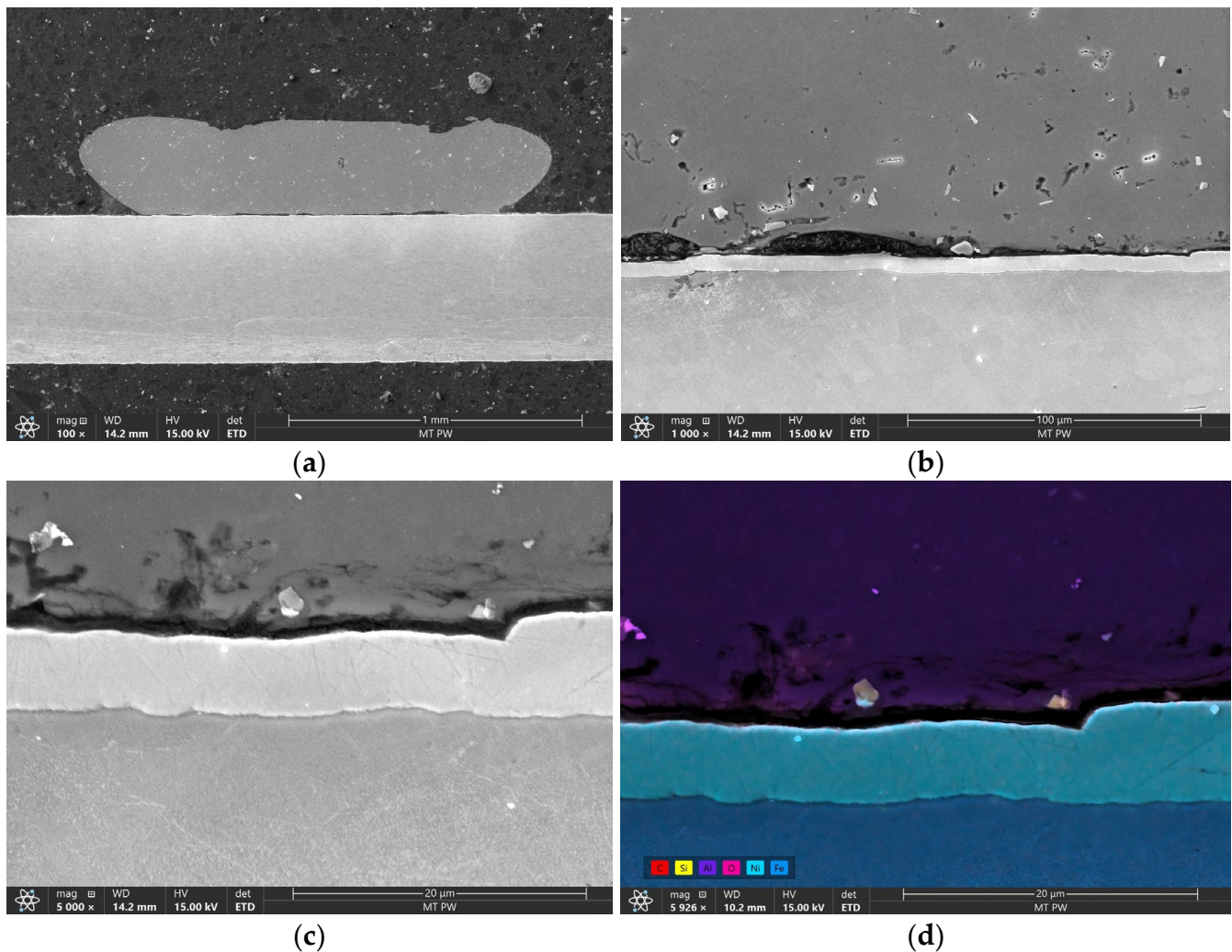


Figure 12. SEM images of the bonded wire on uncleaned sample cross section in 100× (a), 1000× (b), 5000× (c) magnification and EDS quantity map of the sample (d).

Count maps of the elements detected during the EDS analysis for this sample have been presented in Figure 13a–f. This revealed elevated concentrations of carbon, oxygen, and silicon. The elevated presence of carbon might be associated with the mounting powder penetration of the voids in the interface area during the mounting process and silicon can be associated with sample polishing. The oxygen map revealed a high amount of this element not only in the void between the materials but also in the material of the aluminum wire. This is probably due to contamination of the substrate surface that penetrated into the wire during the bonding process.

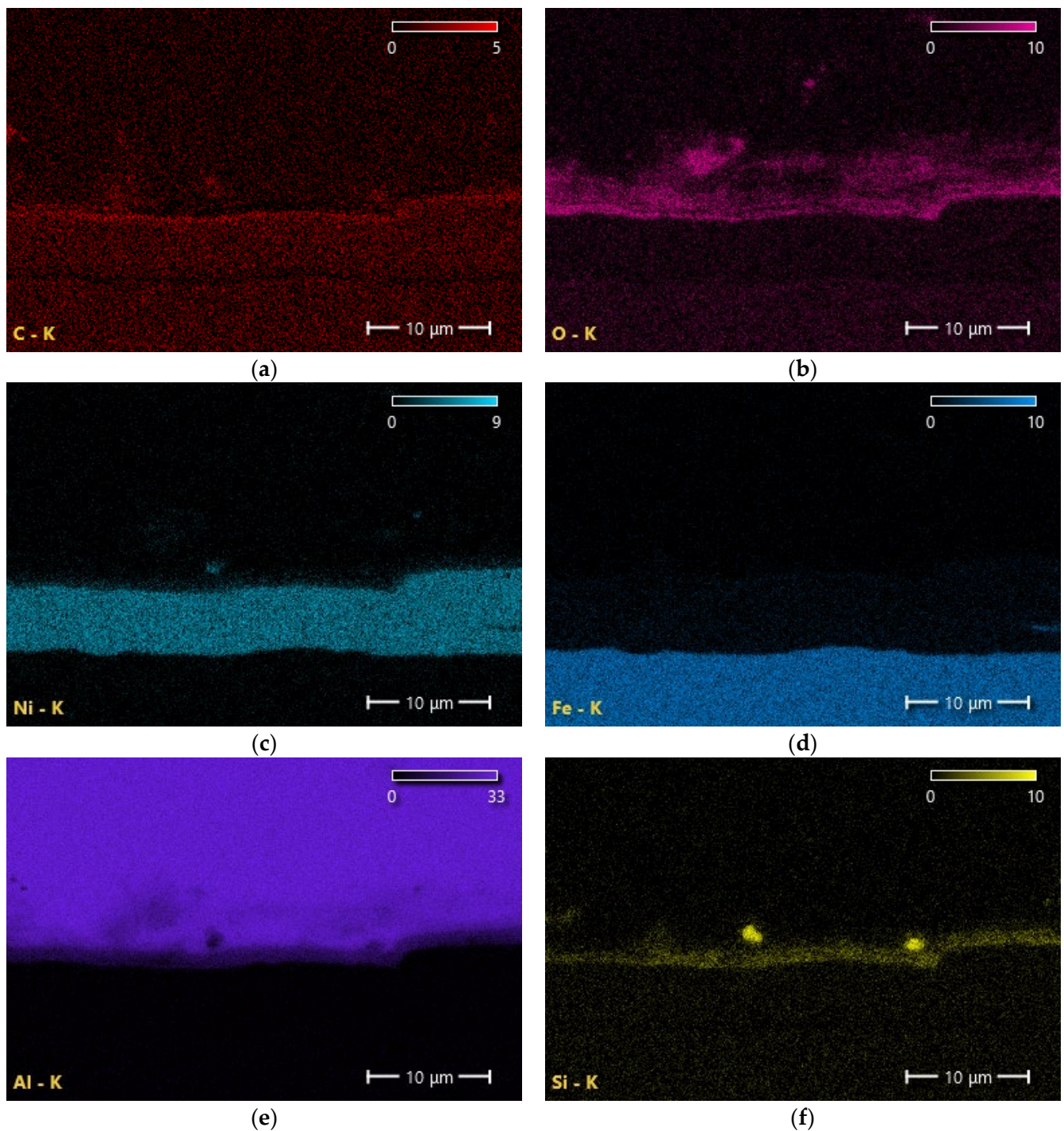


Figure 13. EDS count map of the uncleaned sample bond cross section distribution of carbon (a), oxygen (b), nickel (c), iron (d), aluminum (e), and silicon (f).

Cross sections of the sample made on the surface cleaned with 40% of the laser power seen in Figure 14a–c revealed a few small voids in the interface area. The voids were far smaller than on the uncleaned sample. Figure 14d shows quantity map of elements distribution within the sample measured by means of EDS.

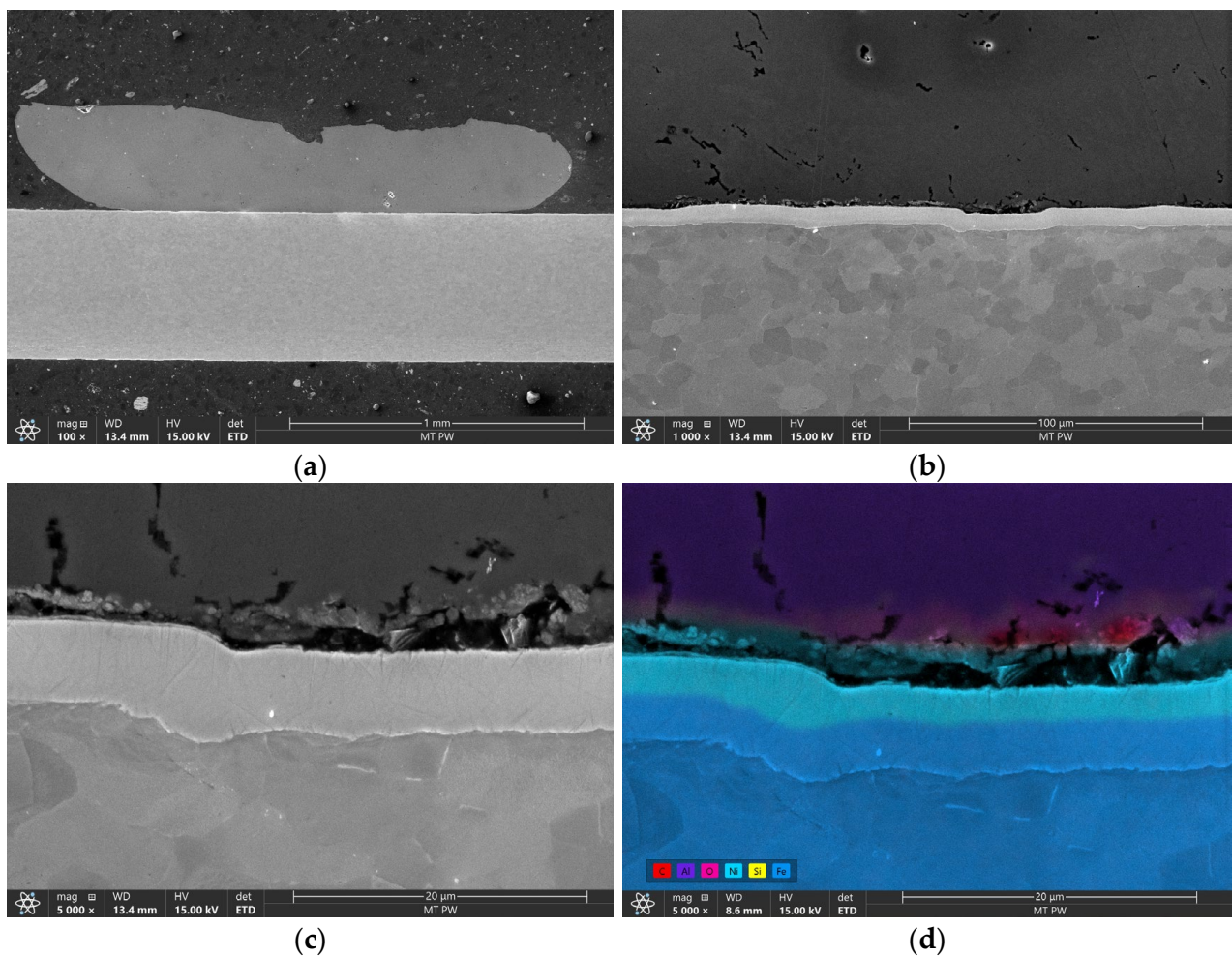


Figure 14. SEM images of the bonded wire on 40% laser power cleaned sample cross section in 100× (a), 1000× (b), 5000× (c) magnification and EDS quantity map of the sample (d).

Count maps of the elements detected during the EDS analysis of the 40% laser cleaned sample cross section seen in Figure 15a–f revealed elevated levels of oxygen in the area of the voids, but they did not penetrate to the aluminum wire material. This indicates that the laser cleaning process has removed the oxides from the substrate surface and had a positive impact on the wire bonding process.

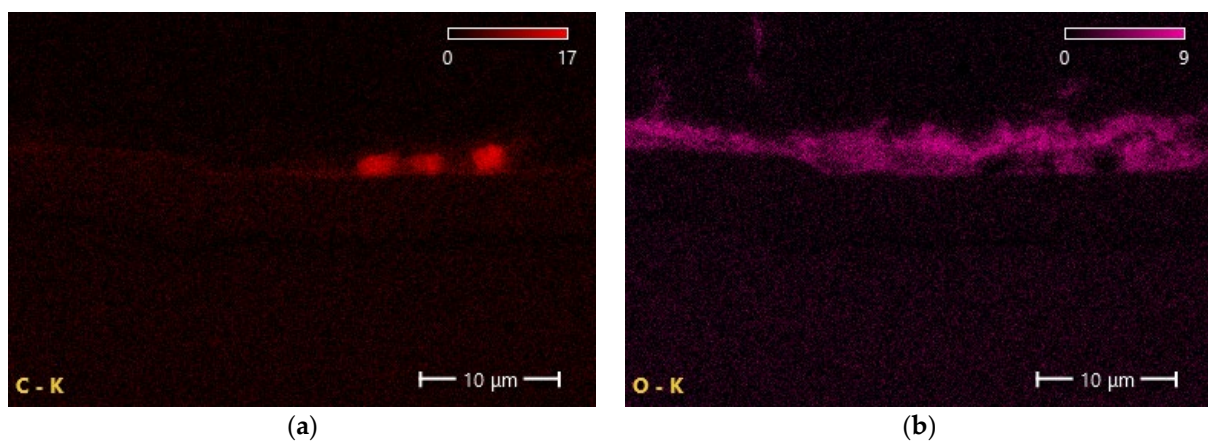


Figure 15. Cont.

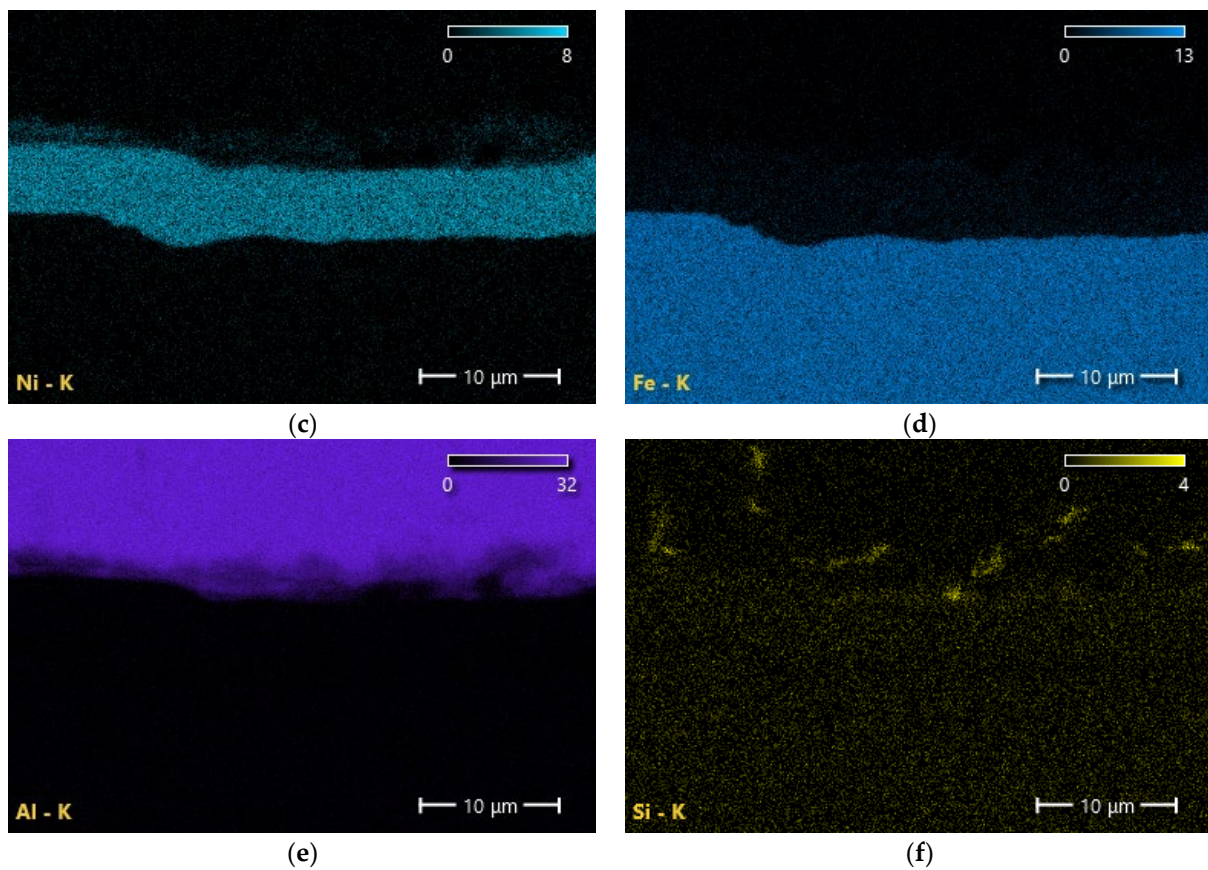


Figure 15. EDS count map of the 40% laser power cleaned sample bond cross section distribution of carbon (a), oxygen (b), nickel (c), iron (d), aluminum (e), and silicon (f).

SEM imaging of the bond cross section sample for 80% of laser power cleaning seen in Figure 16a–c revealed no visible voids in the interface area. This is a very promising result and surface cleaning with this level of laser power should be considered in the process. Figure 16d shows quantity map of elements distribution within the sample measured by means of EDS.

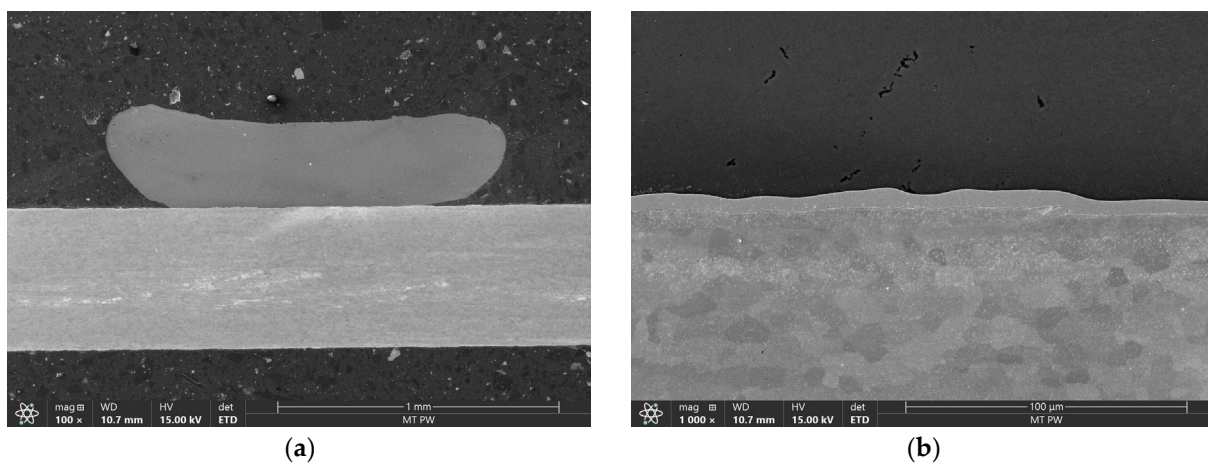


Figure 16. Cont.

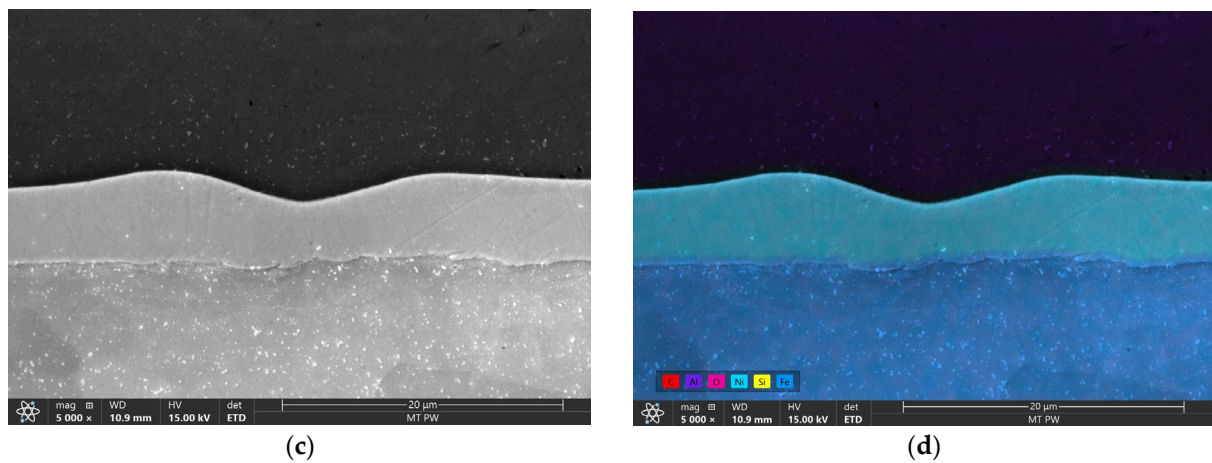


Figure 16. SEM images of the bonded wire on 80% laser power cleaned sample cross section in $\times 100$ (a), $\times 1000$ (b), $\times 5000$ (c) magnification, and EDS quantity map of the sample (d).

Count maps of elements measured using EDS seen in Figure 17a–f reveal no elevated levels of carbon, oxygen, or silicon in the interface area. This indicates good continuity of the interface and confirms the positive influence of surface laser cleaning on the wire bonding process for selected materials.

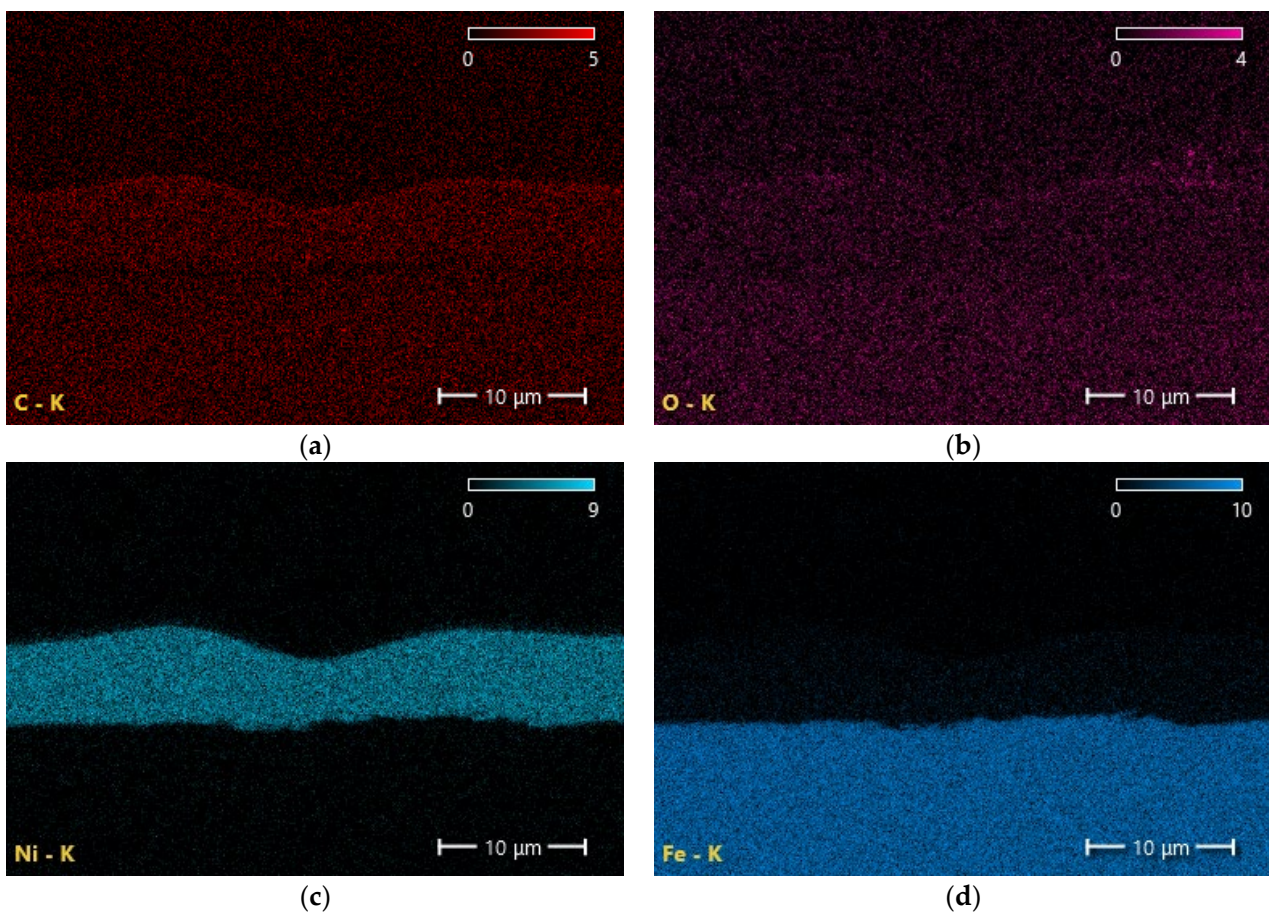


Figure 17. Cont.

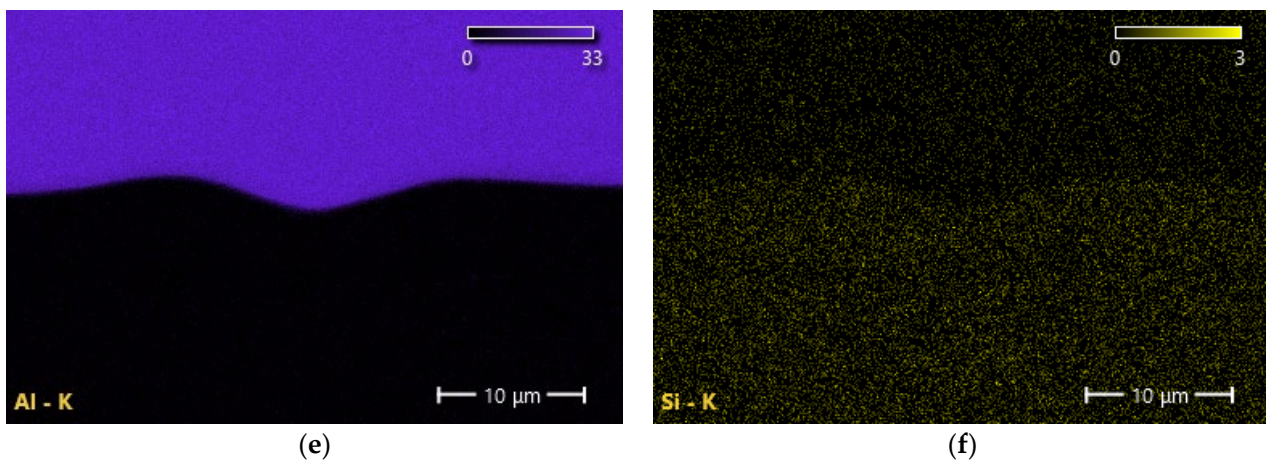


Figure 17. EDS count map of the 80% laser power cleaned sample bond cross section distribution of carbon (a), oxygen (b), nickel (c), iron (d), aluminum (e), and silicon (f).

3.4. Shear Test Results

In order to determine the mechanical properties of the joint shear testing has been conducted on the number of samples.

Force plots measured for the uncleaned bond sample seen on Figure 18 show high variation in the force curve shape indicating different failure modes of the joint.

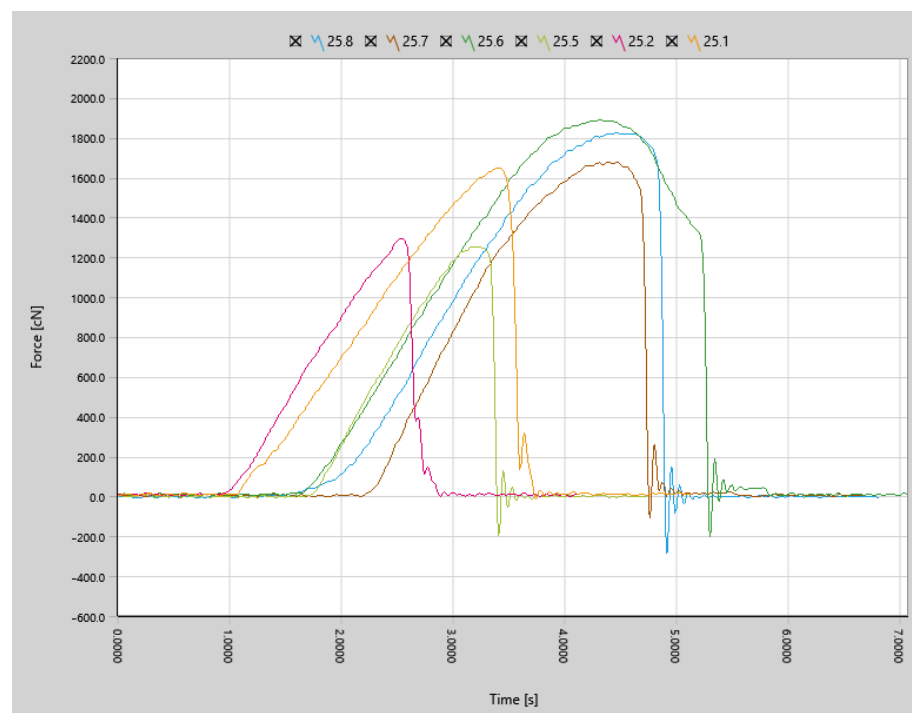


Figure 18. Shear test force plots for 6 samples without laser cleaning.

To further investigate the failure modes of the bonds during shear testing, light macroscopic photos have been taken. Bonds visible in Figure 19a,c show bond liftoff occurred in half of the bond area with the rest of the material being sheared at the shear line. Bonds visible in Figure 19b,d–f experienced full lift off of the wire. Those results indicate no proper nugget formation, poor bonding process performance, and low repeatability of the process.

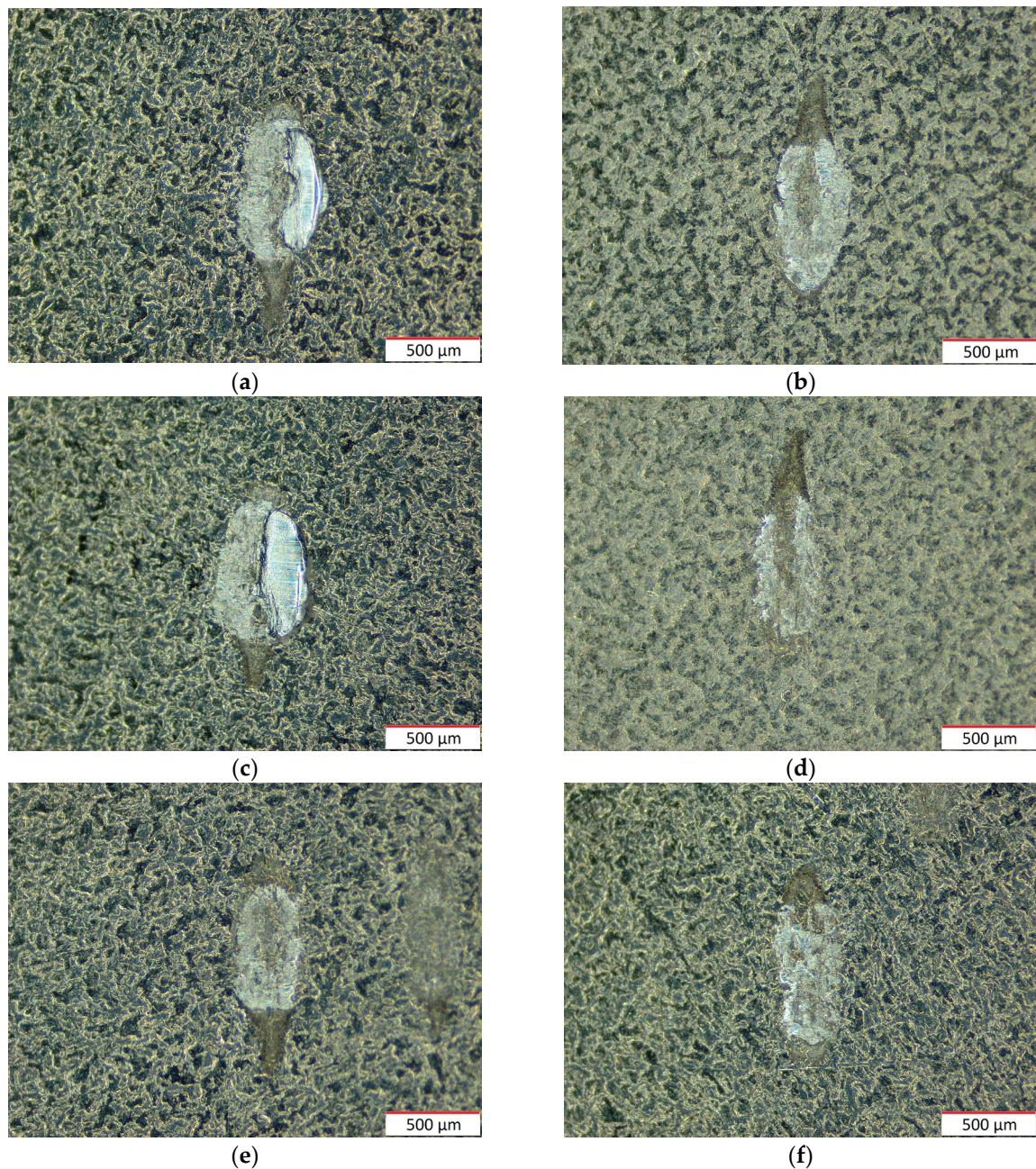


Figure 19. Bonded nugget after shear testing for samples without laser cleaning with $45\times$ magnification of samples 1–6 (a–f).

Numerical results of the shear tests presented in Table 6 revealed that the median of the peak shear force was 1657.5 cN with a standard deviation of 16.1%. This points to the instability of the bonding process confirming a necessity for surface preparation prior to the wire bonding process conducted on cylindrical battery cells.

Table 6. Shear test results for 6 samples without laser cleaning.

Sample Number	1	2	3	4	5	6
Force [cN]	1818.9	1672.6	1884.5	1247.8	1286.4	1642.3
Median [cN]	1657.5					
Standard deviation [cN]	267.6					
Standard deviation [%]	16.1					

The shear test performed on the 40% laser-cleaned sample, which force curves have been presented in Figure 20, indicates that cleaning with this power of the laser beam greatly enhances the repeatability of the wire bonding process for the materials used in this study. Curves have a very consistent shape and size.

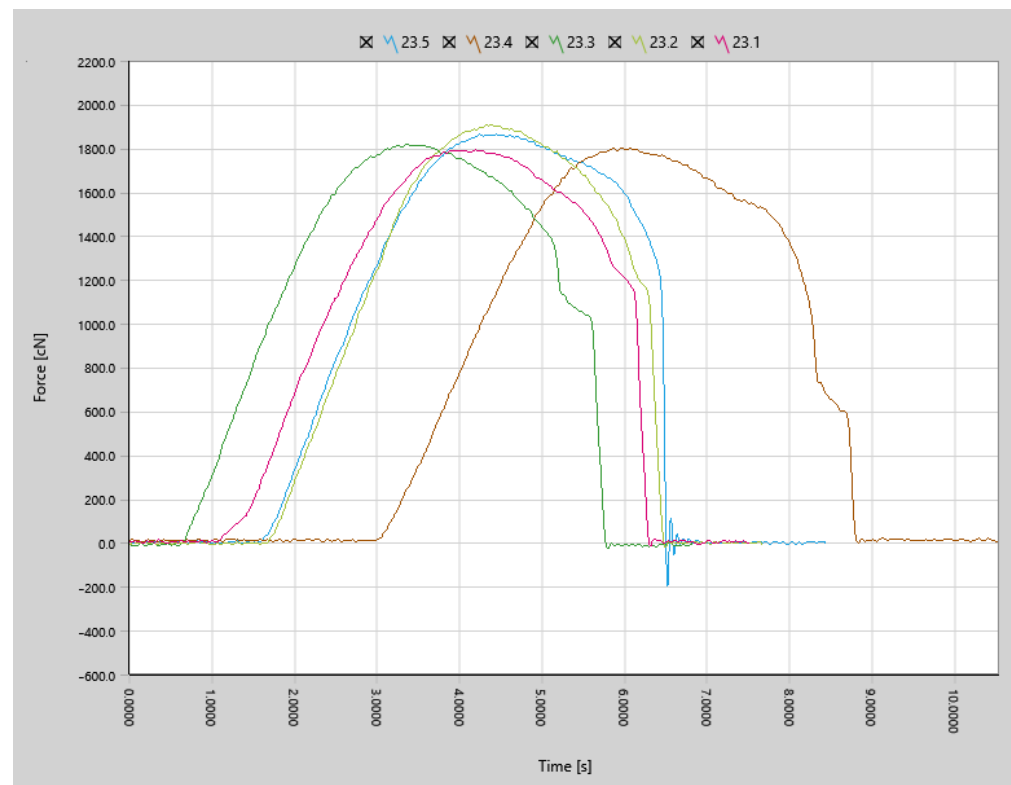


Figure 20. Shear test force plots for 5 samples cleaned with 40% of the laser power.

Light microscopy images presented in Figure 21a–e revealed that the failure mode of the bonds made on the 40% laser-cleaned substrate is the shear of the aluminum wire material on or slightly below the shear line. This points to proper weld nugget formation, especially in the center area of the joint. This kind of failure is highly desired and confirms the positive influence of surface laser cleaning on the wire bonding process.

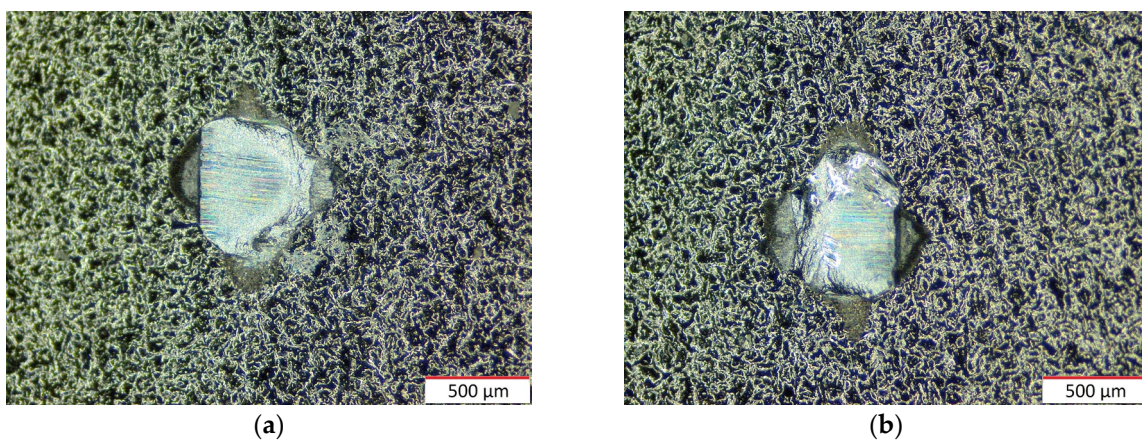


Figure 21. Cont.

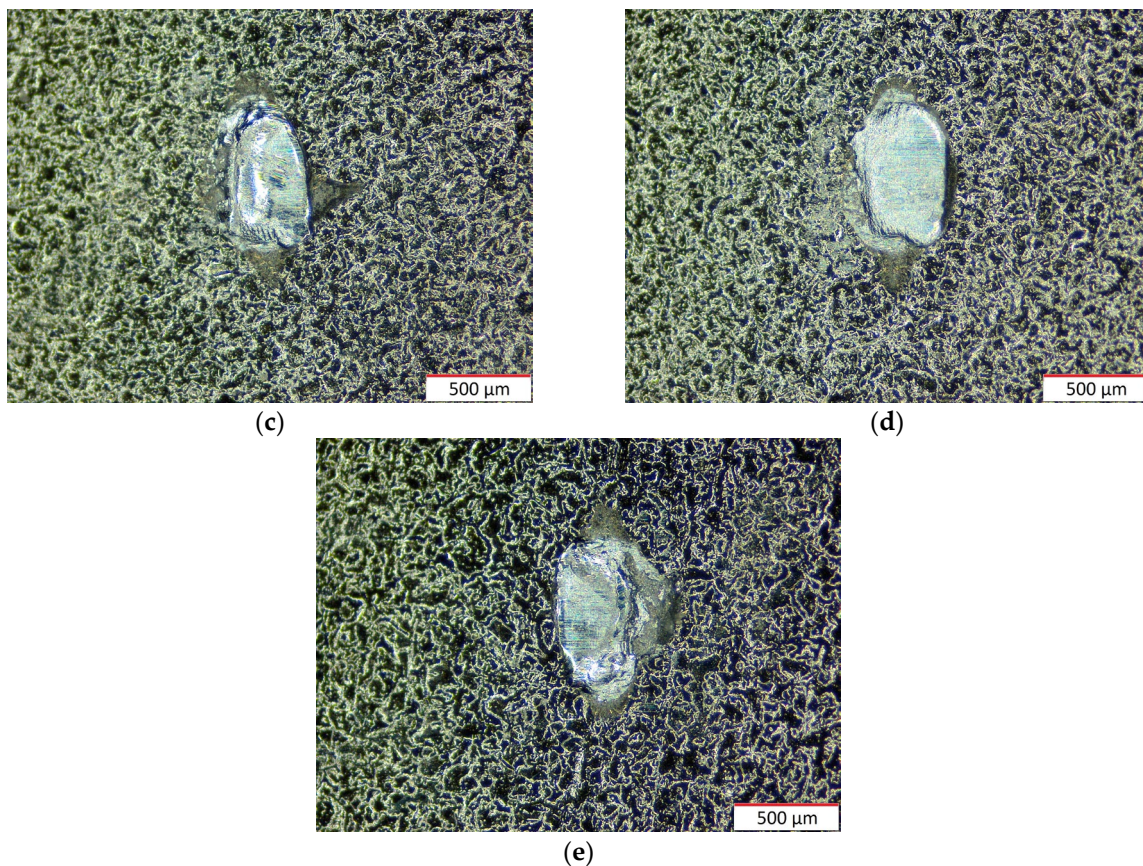


Figure 21. Bond nugget after shear testing for samples with 40% laser cleaning with 45× magnification for samples 1–5 (a–e).

Numerical results of the shear test for the 40% laser power cleaned sample presented in Table 7 show that the median of the peak shear test force was 1814.7 cN with a standard deviation of 2.6%. This is a desired value of force for this pair of materials, while a low standard deviation points to a great improvement in process stability for those cleaning parameters.

Table 7. Shear test results for 5 samples cleaned with 40% of the laser power.

Sample Number	1	2	3	4	5
Force [cN]	1858.6	1796.7	1814.7	1902.1	1786.9
Median [cN]			1814.7		
Standard deviation [cN]			48.0		
Standard deviation [%]			2.6		

Shear test force curves for the 80% laser-cleaned sample have been presented in Figure 22 and are almost identical to the 40% cleaned sample. They are highly repeatable and have very similar shapes.

The macroscopic investigation seen in Figure 23a–e revealed that the failure of bonds occurred at the shear line in the aluminum wire material. This is a great result and indicates proper nugget formation.

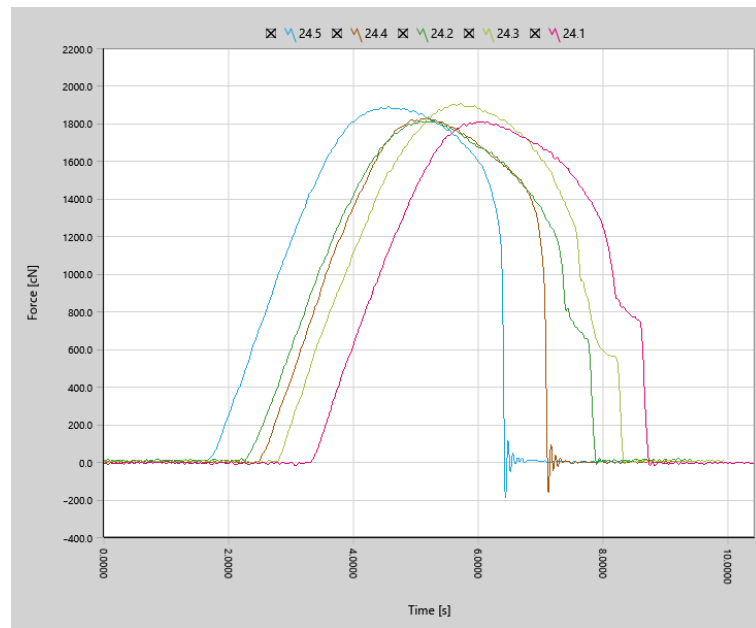


Figure 22. Shear test force plots for 5 samples cleaned with 80% of the laser power.

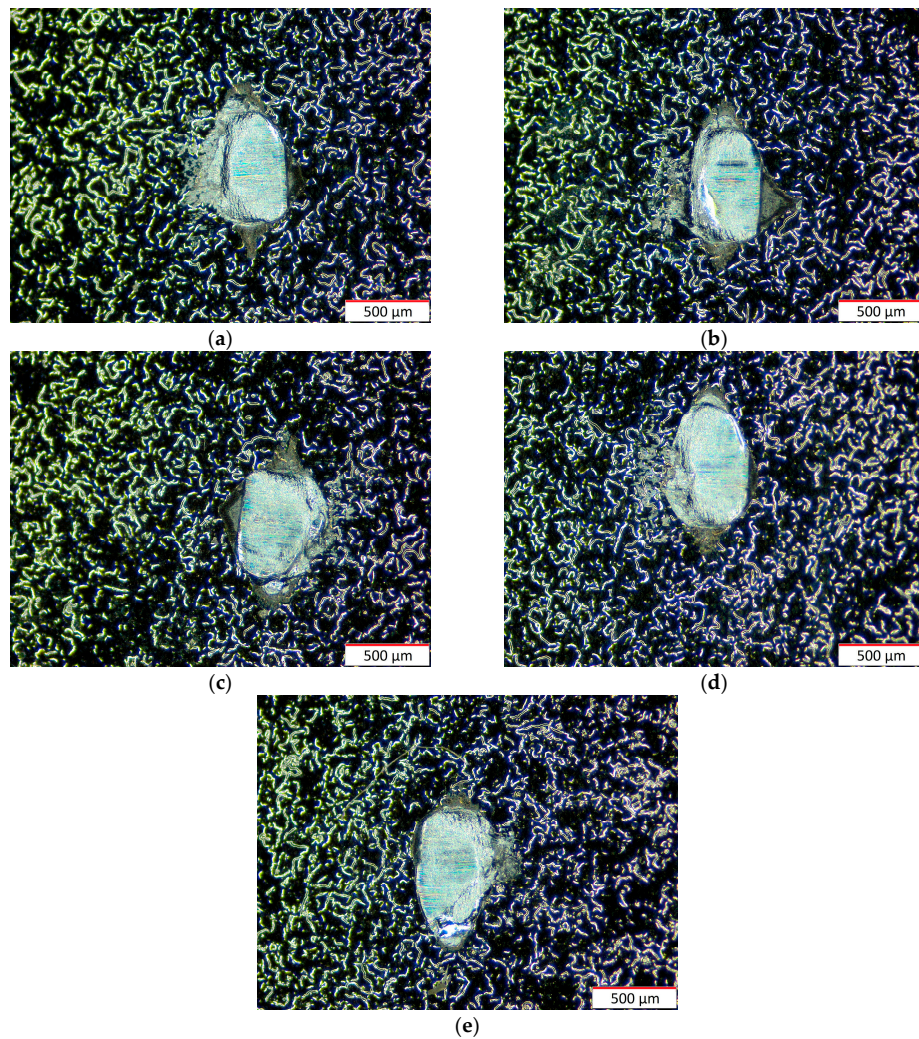


Figure 23. Bond nugget after shear testing for samples with 80% laser cleaning with 45× magnification for samples 1–5 (a–e).

Numerical results of the shear testing for the 80% laser-cleaned sample presented in Table 8 only confirmed high process stability with the median of peak shear force at 1822.6 cN and standard deviation at 2.5%. This result is also very similar to the 40% laser power cleaned sample and indicates no significant impact of raising the laser power on the mechanical properties of the joint.

Table 8. Shear test results for 5 samples cleaned with 80% of the laser power.

Sample Number	1	2	3	4	5
Force [cN]	1886.6	1822.6	1901.1	1805.6	1803.8
Median [cN]			1822.6		
Standard deviation [cN]			46.4		
Standard deviation [%]			2.5		

4. Conclusions

This study confirmed the positive influence of the cylindrical battery surface laser cleaning on the wedge wire bonding process for the parameters and materials used in this study. Laser cleaning with parameters used in this study at 40% laser power shows a positive impact on the joint mechanical properties in the shear test. The joint that was not cleaned before welding has a shear load capacity of a median value of 1657.5 cN and a standard deviation of 267.6 cN (relatively low-level repeatability of the mechanical properties of the joint). After laser cleaning at a power setting of 40%, a shear force with a median value was 1814.7 cN (9.5% increase) and a standard deviation of 48 cN (82% decrease) was obtained. After laser cleaning at an 80% power setting, a shear force with a median value was 1822.6 cN (10% increase) and a standard deviation of 46.4 cN (83% decrease) was obtained.

Additionally, the laser cleaning process greatly reduced the number of oxides in the interface area as indicated by EDS results without significant impact on the nickel plating of the battery case. Cleaning with 80% laser power almost eliminates the oxides from the joint area further improving material contact but did not have an additional impact on the joint mechanical properties and clearly impacts the layer of battery case nickel plating.

Author Contributions: Conceptualization, K.B. and J.Z.; methodology, K.B.; validation, K.B.; formal analysis, K.B.; investigation, K.B.; resources, K.B. and J.Z.; data curation, K.B.; writing—original draft preparation, K.B.; writing—review and editing, K.B. and T.M.C.; visualization, K.B.; supervision, T.M.C.; funding acquisition, J.Z. All authors have read and agreed to the published version of the manuscript.

Funding: This research received no external funding.

Institutional Review Board Statement: Not applicable.

Informed Consent Statement: Not applicable.

Data Availability Statement: Data will be available on e-mail request.

Acknowledgments: We gratefully acknowledge the support provided by Wamtechnik sp. z o.o., Techniczna 2H, and 05-500 Piaseczno, Poland, which provided the wire bonding machine and welding supplies used in this study.

Conflicts of Interest: Jakub Zręda was employed by the company evHive Jakub Zręda. The remaining authors declare that the research was conducted in the absence of any commercial or financial relationships that could be construed as a potential conflict of interest.

References

- Charles, H.K. Advanced wire bonding technology: Materials, methods, and testing. In *Materials for Advanced Packaging*, 2nd ed.; Springer: Boston, MA, USA, 2016; pp. 131–198. [[CrossRef](#)]
- Das, A.; Li, D.; Williams, D.; Greenwood, D. Joining Technologies for Automotive Battery Systems Manufacturing. *World Electr. Veh. J.* **2018**, *9*, 22. [[CrossRef](#)]

3. Eacock, F.; Schaper, M.; Althoff, S.; Unger, A.; Eichwald, P.; Hengsbach, F.; Zinn, C.; Holzweissig, M.J.; Guth, K. Microstructural investigations of aluminum and copper wire bonds. *IMAPSource Proc.* **2014**, *2014*, 845–849. [[CrossRef](#)]
4. Bielizczuk, K.; Zręda, J.; Chmielewski, T. Selected properties of aluminum ultrasonic wire bonded joints with nickel-plated steel substrate for 18650 cylindrical cells. *J. Adv. Join. Process.* **2024**, *9*, 100197. [[CrossRef](#)]
5. Müller, F.; Schiebahn, A.; Reisgen, U. Quality prediction of disturbed ultrasonic metal welds. *J. Adv. Join. Process.* **2022**, *5*, 100086. [[CrossRef](#)]
6. Althoff, S.; Unger, A.; Sextro, W.; Eacock, F. Improving the cleaning process in copper wire bonding by adapting bonding parameters. In Proceedings of the 2015 IEEE 17th Electronic Packaging Technology Conference, EPTC, Singapore, 2–4 December 2015. [[CrossRef](#)]
7. Long, Y.; Dencker, F.; Isaak, A.; Hermsdorf, J.; Wurz, M.; Twiefel, J. Self-cleaning mechanisms in ultrasonic bonding of Al wire. *J. Mater. Process. Technol.* **2018**, *258*, 58–66. [[CrossRef](#)]
8. Lee, S.S.; Shao, C.; Kim, T.H.; Hu, S.J.; Kannatey-Asibu, E.; Cai, W.W.; Spicer, J.P.; Abell, J.A. Characterization of ultrasonic metal welding by correlating online sensor signals with weld attributes. *J. Manuf. Sci. Eng.* **2014**, *136*, 051019. [[CrossRef](#)]
9. Buckmuller, P.; Eberhardt, W.; Kessler, U.; Willeck, H.; Kuck, H. Aluminium wedge-wedge wire bonding on thermoplastic substrates made by LPKF-LDS® technology. In Proceedings of the 3rd Electronics System Integration Technology Conference, ESTC, Berlin, Germany, 13–16 September 2010. [[CrossRef](#)]
10. Zwicker, M.; Moghadam, M.; Zhang, W.; Nielsen, C. Automotive battery pack manufacturing—A review of battery to tab joining. *J. Adv. Join. Process.* **2020**, *1*, 100017. [[CrossRef](#)]
11. Eacock, F.; Unger, A.; Eichwald, P.; Grydin, O.; Hengsbach, F.; Althoff, S.; Schaper, M.; Guth, K. Effect of Different Oxide Layers on the Ultrasonic Copper Wire Bond Process. In Proceedings of the 2016 IEEE 66th Electronic Components and Technology Conference, Las Vegas, NV, USA, 31 May–3 June 2016; pp. 2111–2118. [[CrossRef](#)]
12. Kromer, R.; Costil, S.; Verdy, C.; Gojon, S.; Liao, H. Laser surface texturing to enhance adhesion bond strength of spray coatings—Cold spraying, wire-arc spraying, and atmospheric plasma spraying. *Surf. Coat. Technol.* **2018**, *352*, 642–653. [[CrossRef](#)]
13. Alfano, M.; Pini, S.; Chiodo, G.; Barberio, M.; Pironi, A.; Furgiuele, F.; Groppetti, R. Surface Patterning of Metal Substrates through Low Power Laser Ablation for Enhanced Adhesive Bonding. *J. Adhes.* **2014**, *90*, 384–400. [[CrossRef](#)]
14. Jahani, H.R.; Moffat, B.; Mueller, R.; Fumo, D.; Duley, W.; North, T.; Gu, B. Excimer laser surface modification of coated steel for enhancement of adhesive bonding. *Appl. Surf. Sci.* **1998**, *127–129*, 767–772. [[CrossRef](#)]
15. Jackson, D. CO₂ Spray Cleaning and Osee Non-Contact Inspection for Wire Bond Pad Preparation. *Int. Symp. Microelectron.* **2014**, *2014*, 307–312. [[CrossRef](#)]
16. Chan, Y.H.; Kim, J.-K.; Liu, D.; Liu, P.; Cheung, Y.-M.; Ng, M.W. Effect of plasma treatment of Au-Ni-Cu bond pads on process windows of Au wire bonding. *IEEE Trans. Adv. Packag.* **2005**, *28*, 674–684. [[CrossRef](#)]

Disclaimer/Publisher’s Note: The statements, opinions and data contained in all publications are solely those of the individual author(s) and contributor(s) and not of MDPI and/or the editor(s). MDPI and/or the editor(s) disclaim responsibility for any injury to people or property resulting from any ideas, methods, instructions or products referred to in the content.